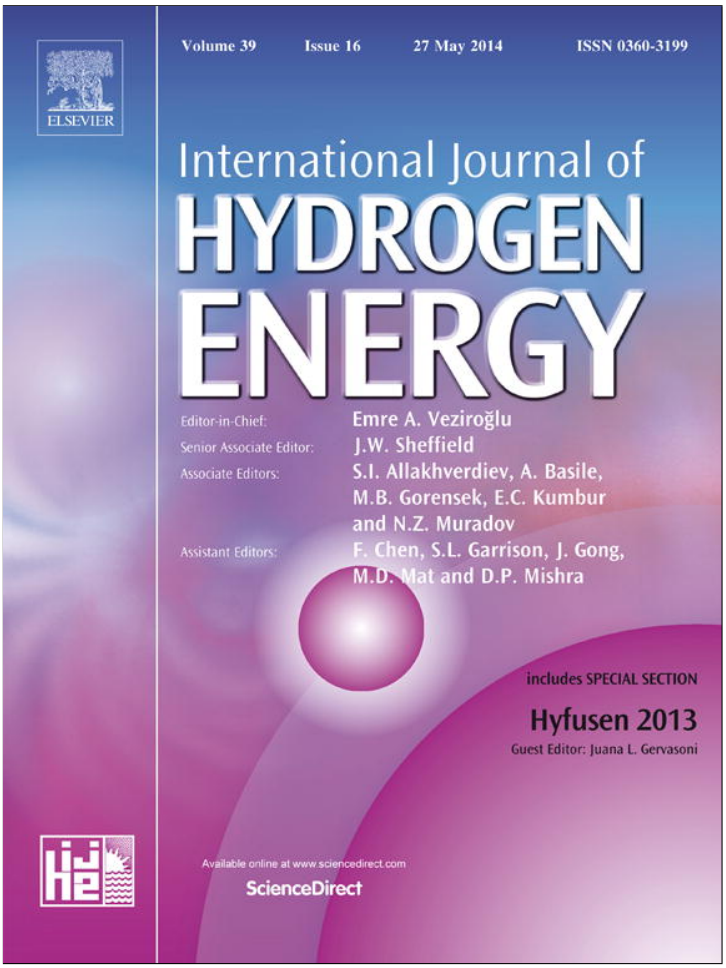

INTERNATIONAL JOURNAL OF HYDROGEN ENERGY 39 (2014) 8744–8748

Available online at www.sciencedirect.com

ScienceDirect

journal homepage: www.elsevier.com/locate/he

Density Functional Theory study of the hydrogen storage in a vacancy zone of an iron–nickel cell

G. Canto [a,1], I. Salazar-Ehuan [a,1], J. González-Sánchez [a,1], A. Tapia [b], R. Quijano [c], S. Simonetti [d,e,*,2]

[a] Universidad Autónoma de Campeche, Av. Agustín Melgar s/n Col. Buenavista, 24039 San Francisco de Campeche, Mexico

[b] Facultad de Ingeniería, Universidad Autónoma de Yucatán, Av. Industrias no Contaminantes, Periférico Norte, Cordemex, A.P. 150, Mérida C.P. 97310, Yucatán, Mexico

[c] Laboratory of Pharmaceutical Chemistry, Faculty of Chemistry, Autonomous University of Yucatan, 41 No. 421 Col. Industrial, C.P. 97150 Mérida, Yucatán, Mexico

[d] Universidad Tecnológica Nacional, 11 de Abril 461, 8000 Bahía Blanca, Argentina

[e] Universidad Nacional del Sur – IFISUR, CONICET, Av. Alem 1253, 8000 Bahía Blanca, Argentina

ARTICLE INFO

Article history:
Received 17 October 2013
Accepted 5 December 2013
Available online 6 January 2014

Keywords:
Iron
Nickel
Hydrogen
Vacancy
DFT
Modeling study

ABSTRACT

Calculations using the SIESTA code have been performed to study the location of one and two hydrogens in a vacancy zone of a $Fe_{50}Ni_{50}$ cell. H debilitates the original metal–metal bonds by forming strong interactions with the metallic matrix. The Fe–H interaction is stronger than the Ni–H interaction. The H–metal exchange contributes to this process. After first H atom adsorption, the strength of the nearest Fe–Fe, Fe–Ni and Ni–Ni bonds decreases to about 89%, 15% and 1%, respectively. Then, the Fe–Fe bond is the most affected. The adsorption of an additional H atom modified the metal–metal strength in a lesser percent. Then, no additional decohesion is observed in the metallic bonds when two H atoms are present but in this case more metallic bonds are affected. The H–H interaction is small; an H_2 molecule is not formed in the vacancy zone of the $Fe_{50}Ni_{50}$ cell.

1. Introduction

Nickel and iron-based alloys are used for high-temperature industrial devices. These materials are sensitive to substances in the operating atmosphere such as hydrogen or water vapor, so that atmospheric degradation [1]. Extensive experimental studies have been conducted to clarify the process but the effect of hydrogen on the material behavior is very complicated; thus, so far no definitive H mechanism on iron–nickel alloys has been established.

Hydrogen introduced by cathodic charging appears to have a significant embrittling effect, measured by a loss of strain to fracture and by the extent of intergranular fracture, for all

* Corresponding author. Universidad Nacional del Sur – IFISUR, CONICET, Av. Alem 1253, 8000 Bahía Blanca, Argentina. Tel.: +54 291 4595141; fax: +54 291 4595142.
E-mail address: ssimonet@uns.edu.ar (S. Simonetti).
[1] Tel.: +52 981 8119800x62800.
[2] Tel.: +54 291 4555220.

0360-3199/$ – see front matter
http://dx.doi.org/10.1016/j.ijhydene.2013.12.039

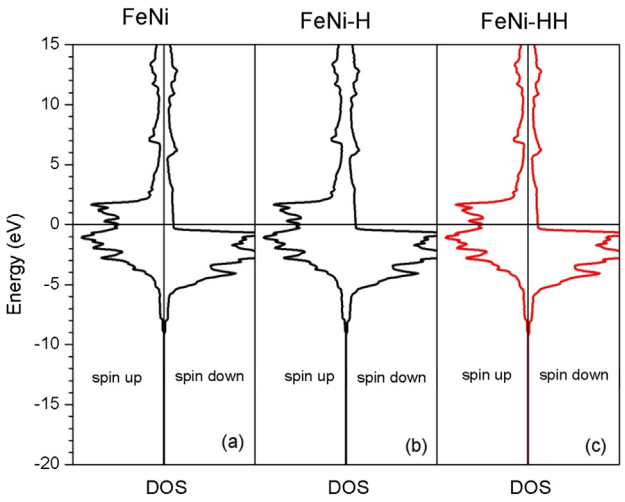

Fig. 1 – DOS of the $Fe_{50}Ni_{50}$ cell, (a) without hydrogen, and containing (b) one and (c) two hydrogen atoms, respectively.

compositions in the FCC gamma-phase region of the Ni–Fe alloy system. The susceptibility of the alloys to hydrogen embrittlement appears to be least for the 50 pct Ni-50 pct Fe alloy and for pure Ni [2].

The reaction of iron–nickel alloys with water depends on pressure. It was found that the amount of hydride formed by the reaction is smaller in the iron–nickel–water system than in the iron–water system, although the hydrogen content in iron–nickel hydride is not significantly different from that in iron hydride. The results indicate that the existence of nickel in iron tend to reduce the amount of hydrogen supplied [3]. In pure nickel, a low hydrogen content caused strain localization only, while a high hydrogen content caused microvoid formation as well. The specimen contains a thin layer of hydride fractured and exhibited brittleness [4].

A study about the dependence of the rate of the production of biogas upon the concentration of nickel and iron at subtoxic concentration and monitored its composition as amount of hydrogen showed that during the acidogenesis phase, nickel reduces, while iron increases, the percentage of dihydrogen in the biogas [5].

Metal–metal and hydrogen–metal energies in hydrogen-free and hydrogen-charged FCC iron, nickel, and iron–nickel alloys have been calculated by ab initio methodology. It is shown that short-range decomposition of Fe–Ni solid solution and difference in Fe–H and Ni–H bonds are responsible for splitting of γ reflections in the X-ray diffraction patterns, which is at variance with the common interpretation in terms of a hydrogen-caused γ^* phase. X-ray diffraction

Table 1 – Distances and energies for the $Fe_{50}Ni_{50}$ cell containing hydrogen.

System	Atom	Distance to the vacancy (Å)	Bond energy (eV/atom)
FeNi–H	H	1.05	2.55
FeNi–HH	H_I/H_{II}	1.09	2.59

Table 2 – Overlap population (OP) of the H–metal interactions.

System	Bond	Distance (Å)	OP
FeNi–H	H_I–Fe_I	1.76	0.133
	H_I–Ni_I	2.70	0.018
FeNi–H H	$H_{I/II}$–$Fe_{I/II}$	1.73	0.138
	$H_{I/II}$–$Ni_{I/II}$	2.72	0.014
	H_I–H_{II}	2.18	0.007

measurements confirm the absence of miscibility gap in the FeNi–H solid solution and its occurrence in Ni–H. Results of calculations are consistent with the absence of H–H pairs in pure nickel [6].

Other effect of hydrogen on fracture is that it causes a decrease in the atomic bond strength, e.g., decohesion. H is predicted to weaken the atomic bonding. On the other hand, hydrogen atoms in metals tend to concentrate in defects of the crystal structure. Vacancy contributions to hydrogen embrittlement and hydrogen-induced degradation of mechanical properties have been interesting issues especially in steels [7].

In this research we study the effect on the metal–metal bonding, of one and two hydrogens located in a vacancy region of an FCC $Fe_{50}Ni_{50}$ alloy. We calculate the electronic structure and bonding during the adsorption phenomena. We also analyze the possibility of forming an H_2 molecule in the $Fe_{50}Ni_{50}$ alloy.

2. Results and discussions

The calculations were performed with a DFT based code using a Linear Combination of Atomic Orbitals and considering pseudopotentials for the core electrons as implemented in the SIESTA code [8–15]. A slab constituted by 232 atoms, Fe and Ni metal atoms (50:50) distributed in six close-packed FCC (111)

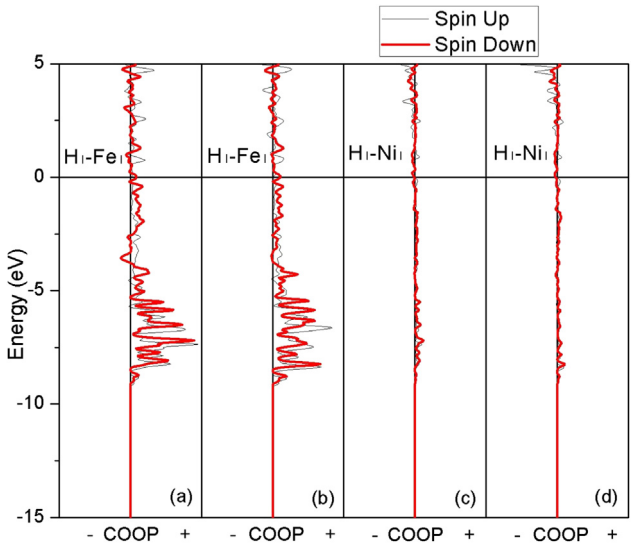

Fig. 2 – COOP curves of the hydrogen–metal interactions, (a) and (c) in the $Fe_{50}Ni_{50}$–H system, (b) and (d) in the $Fe_{50}Ni_{50}$–H–H system.

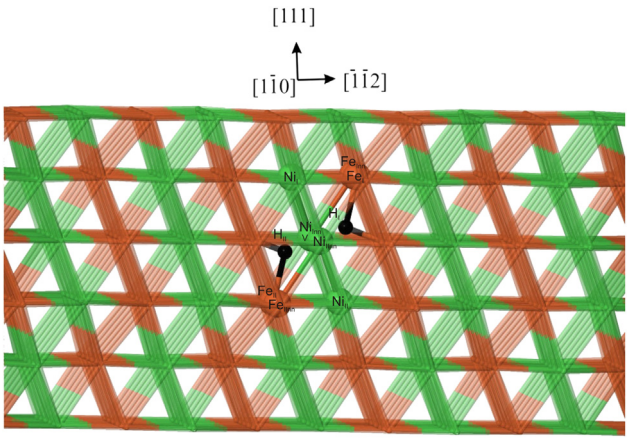

Fig. 3 – A schematic view of the $Fe_{50}Ni_{50}$ cell containing the H pair. The atoms that participate in the interactions and the vacancy (V) are labeled.

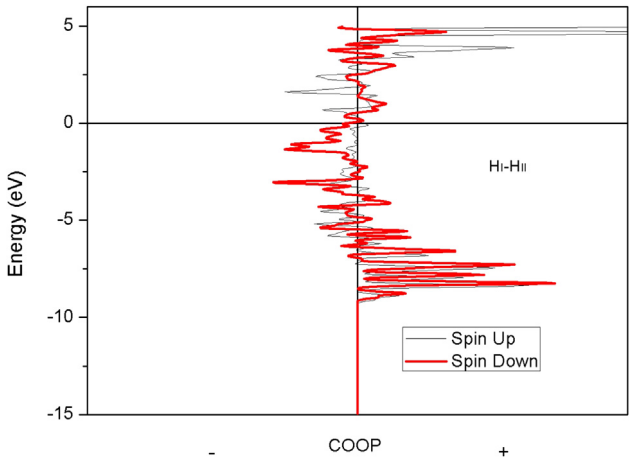

Fig. 4 – COOP curve of the H–H interaction.

planes, is used to represent a vacancy and its environment. Initial metal bond lengths were taken at the bulk value of 2.54 Å and the distance between planes was 2.074 Å. We have study the isolated $Fe_{50}Ni_{50}$ system, and containing one and two H atoms, respectively, located in the vacancy region of the $Fe_{50}Ni_{50}$ alloy. The initial geometry for an isolated H and an H–H pair in the vacancy was taken from previous semi-empirical calculations [16]. A geometry optimization was performed applying relaxation calculations. In Fig. 1 is showed the density of states (DOS) of all the studied systems. The hydrogen sorption is not perceived in Fig. 1(b) and (c) because the H low concentration. The value of the Fermi energy is positioned at 0 eV and it changes slightly after H adsorption. Table 1 shows the H-vacancy distance and energy for each system by SIESTA calculations. As we can see, the energy of two H atoms with one vacancy is very close to the energy of one H atom with a vacancy. The system containing two hydrogens is a little more stable than the other one, the energy difference is only 0.09 eV. That means that the hydrogen's prefer to be associated forming a vacancy-H–H (VH_2) cluster rather than alone. Studies concerning H accumulation in vacancies showed that VH_2 system is the most favorable for pure BCC Fe and FCC FeNi alloy [16,17]. When two H are present, the H-vacancy distance is little bigger (0.04 Å) comparing with the system containing one hydrogen atom, and is in agreement with getting less repulsion between the hydrogens. On the other hand, the H atoms locate nearer Fe atoms than Ni atoms resulting an H–Fe overlap population (OP) bigger than the H–Ni OP (see Table 2). A view of H–metal OP interactions can be seen in Fig. 2, where a noticeable bigger H–Fe interaction is detected. A schematic view of the H–H location in the vacancy region of the $Fe_{50}Ni_{50}$ alloy is showed in Fig. 3. For the final configuration, we found an H–H distance of 2.18 Å. Typical H_2 bond is not formed in the $Fe_{50}Ni_{50}$ vacancy because the calculated H–H distance is longer than in the free H_2 molecule (0.74 Å). A very little interaction arises between the hydrogen atoms because same antibonding states are filled resulting a small H–H OP (see Fig. 4). This analysis is important in order to check the possible formation of a molecular hydrogen bubble in the vacancy region of the $Fe_{50}Ni_{50}$ alloy from which cracks may start to weaken the metal. This embrittlement category is also responsible for failures in hydrogen-related process plants, a phenomenon known as 'Hydrogen attack'.

The H bonds with nearest neighbors Ni and Fe atoms. The H–Fe and H–Ni interactions are developed while the Fe–Fe, Ni–Ni and Ni–Fe bond strength decrease. The metal–metal strength changes, due to the local concentration of H, are evidenced. After one H atom adsorption, the strength of the nearest Fe–Fe, Fe–Ni and Ni–Ni bonds decreases to about 89%, 15% and 1% (see Table 3). The adsorption of an additional H modified the metal–metal bond strength in a lesser percent. The Fe–Fe OP increases between 1.22% and 6.40%, the Ni–Ni OP decreases between 0.9% and 3.5% while the Ni–Fe OP changes between 0.9% and 13.44%. In general, the adsorption

Table 3 – Overlap population (OP) of the metal–metal interactions.

Bond	FeNi		FeNi–H		FeNi–H H	
	Distance (Å)	OP	Distance (Å)	OP	Distance (Å)	OP
Fe_I–Fe_{Inn}	2.54	0.730	2.53	0.082	2.53	0.083
Fe_{II}–Fe_{IInn}	2.54	0.730	2.54	0.078	2.53	0.083
Ni_I–Ni_{Inn}	2.50	0.115	2.50	0.114	2.52	0.110
Ni_{II}–Ni_{IInn}	2.51	0.114	2.51	0.111	2.52	0.110
Fe_I–Ni_I	2.46	0.121	2.48	0.103	2.48	0.104
Fe_{II}–Ni_{II}	2.46	0.121	2.46	0.119	2.49	0.103

nn = nearest neighbor.

of an additional H does not increase the decohesion percent; therefore, more metallic bonds are affected. The COOP curves for the metal–metal interactions are shown in Fig. 5. After one H adsorption, the more noticeable detrimental effect is observed in the Fe–Fe bonds; while after the second H location, the Fe–Ni bond is the most affected. Our results show how H locates near a vacancy decreasing the bond strength of the neighboring metallic bonds and contributing to the decohesion process.

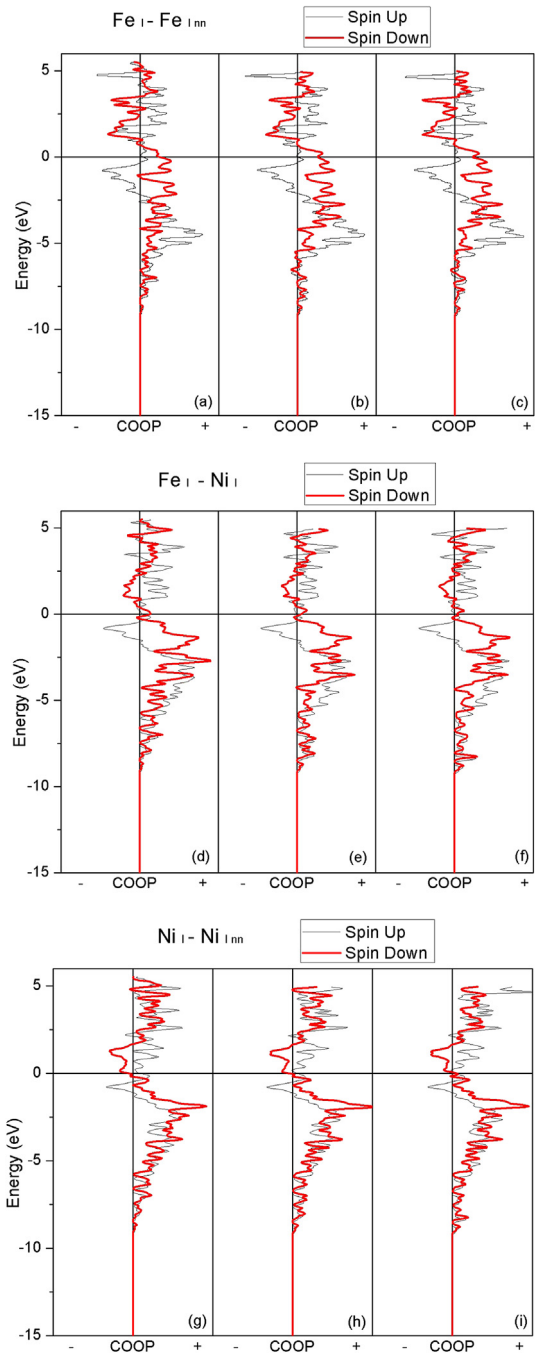

Fig. 5 – COOP curves for the metal–metal interactions in the $Fe_{50}Ni_{50}$ cell, (a), (d) (g) without hydrogen; (b), (e) (h) containing one hydrogen and (c) (f) (i) containing two hydrogen atoms.

Table 4 – Net charge of the atoms that participate in the interactions.

System	Atom	Net charge (e^-)	
		Bader	DDEC/C3
FeNi	Fe_I	0.261	0.099
	Fe_{Inn}	0.211	0.072
	Ni_I	−0.296	−0.094
	Ni_{Inn}	−0.208	−0.064
	Fe_{II}	0.262	0.098
	Fe_{IInn}	0.211	0.069
	Ni_{II}	−0.253	−0.093
	Ni_{IInn}	−0.242	−0.064
FeNi–H	Fe_I	0.330	0.105
	Fe_{Inn}	0.252	0.076
	Ni_I	−0.276	−0.069
	Ni_{Inn}	−0.224	−0.050
	Fe_{II}	0.250	0.092
	Fe_{IInn}	0.250	0.065
	Ni_{II}	−0.231	−0.071
	Ni_{IInn}	−0.224	−0.050
	H_I	−0.394	−0.097
FeNi–H H	Fe_I	0.333	0.096
	Fe_{Inn}	0.254	0.070
	Ni_I	−0.261	−0.048
	Ni_{Inn}	−0.208	−0.030
	Fe_{II}	0.335	0.099
	Fe_{IInn}	0.258	0.071
	Ni_{II}	−0216	−0.050
	Ni_{IInn}	−0.208	−0.030
	H_I	−0.402	−0.085
	H_{II}	−0.403	−0.085

We have obtained charge populations following two methodologies based on electronic charge densities. First, the Bader [18,19] procedure was employed using the Tang implementation [20–22]. Second, the Density Derived Electrostatic and Chemical (DDEC) method developed by Manz [23,24] was also employed in order to get charge populations that reproduce the electrostatic potential outside the electron distribution. Table 4 shows the populations obtained, despite the magnitude of charge are different, the ionic character on each chemical species has the same sign. The Bader charges greater than the DDEC/c3 charges is a known behavior when a comparison between them is performed [23,24]. In general both methods shows a negative charge for hydrogen mainly taken from Iron and secondly from Nickel nearest neighbor. However, both chemical species, Fe and Ni, retain the same net polarization as in FeNi bulk.

3. Conclusions

DFT calculations have been performed to study the effect of one and two H located in a vacancy region of a $Fe_{50}Ni_{50}$ alloy.

The H impurities develop a negative charge while the closest Fe and Ni atoms result more positively charged. The H–metal exchange contributes to the decohesion process. H debilitates the metal–metal bonds by forming interactions with the metallic matrix. The metal–metal bond strength decreases a bigger percent with the introduction of the first H atom and no additional decohesion is observed in the metallic

bonds when two H atom are present but more bonds are affected. The H–H interaction in the vacancy region is very small. Each H atom bonds to the surrounding Fe and Ni instead of bonding with each other. The Fe–H interaction is stronger than the Ni–H interaction.

Acknowledgments

Our work was supported by the MINCyT-CONACyT Scientific-Technological Cooperation Program (MX/09/11), PIP 0103 (CONICET), PGI 25/B029 (UTN), PGI 24/ZFO3 (UNS). Simonetti is member of CONICET-Argentina.

REFERENCES

[1] Hirth JP. Effects of hydrogen on the properties of iron and steel. Metall Trans A 1980;11:861–90.
[2] Birnbaum HK. Mechanisms of hydrogen related fracture of metals. Metall Trans A 1989;20A:1475–82.
[3] Hirao N, Ohtani E, Kondo T, Kikegawa T. Iron–nickel–water system under high pressure and high temperature. American Geophysical Union; 2004. Fall Meeting, abstract #T41B-1182.
[4] Xu X, Wen M, Fukuyama S, Yokogawa K. Simulation of hydrogen embrittlement at crack tip in nickel single crystal by embedded atom method. Mat Trans 2001;42:2283–9.
[5] Aresta M, Narracci M, Tommasi I. Influence of iron, nickel and cobalt on biogas production during the anaerobic fermentation of fresh residual biomass. Chem Ecol 2003;19:451–9.
[6] Movchan DN, Shyvanyuk VN, Shanina BD, Gavriljuk VG. Atomic interactions and hydrogen-induced gamma phase in fcc iron–nickel alloys. Phys Stat Sol (a) 2010;207:1796–801.
[7] Naguno M. Function of hydrogen in embrittlement of high-strength steels. ISIJ Int 2001;41:590–8 [and reference therein].
[8] Soler JM, Artacho E, Gale JD, Garcia A, Junquera J, Ordejon P, Sanchez-Portal D. The SIESTA method for ab initio order-materials simulation. J Phys Condens Matter 2002;14:2745–79.
[9] Hohenberg P, Kohn W. Inhomogeneous electron gas. Phys Rev 1964;136:B864–71.
[10] Perdew JP, Burke K, Ernzerhof M. Generalized gradient approximation made simple. Phys Rev Let 1996;77:3865–8.
[11] Ordejon P, Artacho E, Soler JM. Self-consistent order-N density-functional calculations for very large systems. Phys Rev B 1996;53:R10441–4.
[12] Sánchez-Portal D, Ordejon P, Canadell E. Computing the properties of materials from first principles with SIESTA. Struct Bond 2004;113:103–70.
[13] Troullier N, Martins JL. Efficient pseudopotentials for plane-wave calculations. Phys Rev B 1991;43:1993–2006.
[14] Sankey OF, Niklewski DJ. Ab initio multicenter tight-binding model for molecular-dynamics simulations and other applications in covalent systems. Phys Rev B 1989;40:3979–95.
[15] Monkhorst HJ, Pack JD. Special points for Brillouin-zone integrations. Phys Rev B 1976;13:5188–92.
[16] Simonetti S, Brizuela G, Juan A. Multiple hydrogen location in a vacancy region of a FCC iron–nickel-based alloy. Mol Phys 2010;108:79–86.
[17] Tateyama Y, Ohno T. Stability and clusterization of hydrogen-vacancy complexes in α-Fe: an ab initio study. Phys Rev B 2003;67:174105-1–174105-10.
[18] Bader R. Atoms in molecules: a quantum theory. New York: Oxford University Press; 1990.
[19] Bader RFW. Principle of stationary action and the definition of a proper open system. Phys Rev B 1994;49:13348–56.
[20] Tang W, Sanville E, Henkelman G. A grid-based Bader analysis algorithm without lattice bias. J Phys Condens Matter 2009;21:084204–7.
[21] Sanville E, Kenny SD, Smith R, Henkelman G. An improved grid-based algorithm for Bader charge allocation. J Comp Chem 2007;28:899–908.
[22] Henkelman G, Arnaldsson A, Jónsson H. A fast and robust algorithm for Bader decomposition of charge density. Comput Mater Sci 2006;36:254–360.
[23] Manz TA, Sholl DS. A dimensionless reaction coordinate for quantifying the lateness of transition states. J Chem Theory Comput 2010;6:2455–68.
[24] Manz TA, Sholl DS. Improved atoms-in-molecule charge partitioning functional for simultaneously reproducing the electrostatic potential and chemical states in periodic and nonperiodic materials. J Chem Theory Comput 2012;8:2844–67.